International Journal of Refrigeration 88 (2018) 538–551

Contents lists available at ScienceDirect

International Journal of Refrigeration

journal homepage: www.elsevier.com/locate/ijrefrig

Horizontal convective boiling of R1234yf, R134a, and R450A within a micro-fin tube

M.A. Kedzierski*, D. Kang

National Institute of Standards and Technology, Gaithersburg, MD 20899, Unites States

ARTICLE INFO

Article history:
Received 27 November 2017
Revised 5 February 2018
Accepted 25 February 2018
Available online 11 March 2018

Keywords:
Boiling
Enhanced heat transfer
Low-GWP
Micro-fin
Refrigerant mixtures

ABSTRACT

This paper presents local convective boiling heat transfer and Fanning friction factor measurements in a micro-fin tube for R134a and two possible low global warming potential (GWP) refrigerant replacements for R134a, namely R1234yf and R450A. Test section heating was achieved with water in either counterflow or in parallel flow with the test refrigerant to provide for a range of heat fluxes for each thermodynamic quality. An existing correlation from the literature for single and multi-component mixtures was shown to not satisfactorily predict the convective boiling measurements for flow qualities greater than 40%. Accordingly, a new correlation was developed specifically for the test fluids of this study so that a fair comparison of the heat transfer performance of the low GWP refrigerants to that of R134a could be made. The new correlation was used to compare the heat transfer coefficient of the three test fluids at the same heat flux, saturated refrigerant temperature, and refrigerant mass flux. The resulting example comparison, for the same operating conditions, showed that the heat transfer coefficient of the multi-component R450A and the single-component R1234yf were, on average, 15% less and 5% less, respectively, than that of the single-component R134a. Friction factor measurements were also compared to predictions from an existing correlation. A new correlation for the friction factor was developed to provide a more accurate prediction. The measurements and the new models are important for the evaluation of potential low-GWP refrigerants replacements for R134a.

Ébullition convective horizontale de R1234yf, R134a, et R450A dans un tube à micro-ailettes

Mots-clés: Ébullition; Transfert de chaleur amélioré; Faible GWP; Micro-ailettes; Mélanges de frigorigènes

1. Introduction[1]

Evaporators and condensers for new unitary refrigeration and air-conditioning equipment typically use internally enhanced tubes, like the micro-fin tube, to provide improved refrigerant-side, two-phase heat transfer performance. The micro-fin tube is a good choice for unitary equipment because it provides the highest heat transfer with the lowest pressure drop of the commercially available internal enhancements (Webb and Kim, 2005). Consequently, flow boiling heat transfer data for the micro-fin tube with R1234yf and R450A are essential for the evaluation of their use for unitary applications.

Pressure from the policies set by the Montreal Protocol (1987) concerning ozone depletion potential (ODP), and the Kyoto Protocol (1997) and the European Mobile Directive (2006) for global warming potential (GWP) have caused a recent shift to refrigerants with both zero ODP and low GWP. Refrigerant R134a, ubiquitously used for air-conditioning and refrigeration applications, has zero ODP, but a rather large 100-year horizon GWP[2]

* Corresponding author.
E-mail address: mark.kedzierski@nist.gov (M.A. Kedzierski).

[1] Certain trade names and company products are mentioned in the text or identified in an illustration in order to adequately specify the experimental procedure and equipment used. In no case does such an identification imply recommendation or endorsement by the National Institute of Standards and Technology, nor does it imply that the products are necessarily the best available for the purpose.

[2] All GWP values are given for zero contribution from climate-carbon feedbacks.

https://doi.org/10.1016/j.ijrefrig.2018.02.021
0140-7007/Published by Elsevier Ltd.

Nomenclature

English symbols

A_c	cross-sectional area (m^2)
Bo	local boiling number, $\frac{q''}{G_r i_{fg}}$
c_p	specific heat (J kg^{-1} K^{-1})
C	coefficients given in Eq. (5)
D_e	equivalent inner diameter of smooth tube, $\sqrt{\frac{4A_c}{\pi}}$ (m)
D_h	hydraulic diameter of micro-fin tube (m)
e	fin height (mm)
f	Fanning friction factor
g	acceleration due to gravity (m/s^2)
G	total mass velocity (kg m^{-2} s^{-1})
$h_{2\phi}$	local two-phase heat-transfer coefficient (W $m^{-2}\cdot K^{-1}$)
i_{fg}	latent heat of vaporization (J kg^{-1})
k	refrigerant thermal conductivity (W m^{-1} K^{-1})
K_f	dimensionless two-phase number defined by Eq. (9)
Nu	local Nusselt number based on D_h
$\dot{m}$	mass flow rate (kg s^{-1})
M_w	molar mass (g $mole^{-1}$)
p	wetted perimeter (m)
P	local fluid pressure (Pa)
Pr	liquid refrigerant Prandtl number $\frac{c_p \mu}{k}\|_{r,l}$
q''	local heat flux based on A_i (W m^{-2})
Re	all liquid, refrigerant Reynolds number based on $D_h = \frac{G_r D_h}{\mu_{r,l}}$
s	distance between fins (mm)
T	temperature (K)
t_b	bottom thickness of fin (mm)
t_w	tube wall thickness (mm)
U	expanded relative uncertainty (%)
x_q	thermodynamic mass quality (-)
z	axial distance (m)

Greek symbols

α	helix angle (°)
β	fin angle (°)
ΔL	incremental length (m)
ΔT_s	T_s - T_w (K)
μ	viscosity (Pa s)
ν	specific volume, $x_q \nu_v + (1 - x_q)\nu_l$ (m^3 kg^{-1})
ρ	density (kg m^{-3})
σ	surface tension (kg s^{-2})

Subscripts

b	bubble point
c	critical condition
d	dew point
f	water
i	inside, inlet
l	liquid
o	outlet, exit
p	prediction, single component
r	refrigerant
s	saturated state
v	vapor
w	heat transfer surface

of 1300 (IPCC, 2013). Two new refrigerants, R1234yf (2,3,3,3-Tetrafluoroprop-1-ene), and R450A (R1234ze/R134a (58/42)), are potential low GWP replacements for R134a having GWPs of < 1 (Myhre et al., 2013) and 547 (Honeywell, 2014), respectively.

A significant number of experimental measurement studies of evaporative heat transfer in the micro-fin tubes have been published for R134a. For example, Olivier et al. (2004), Yun et al. (2002), Seo and Kim (2000), Yu et al. (2002), Kim et al. (2002), Hamilton et al. (2008), and Wellsandt and Vamling (2005) have produced experimental data and/or developed models for R134a flow boiling in a variety of micro-fin tube geometries. The purpose of making measurements with R134a in the present study is to establish an evaporative heat transfer performance baseline that can be used to compare to the low GWP replacements, R1234yf and R450A.

The number of experimental measurement studies of evaporative heat transfer in micro-fin tubes for R1234yf is less extensive than that for R134a. Park and Jung (2010) and Saitoh et al. (2011) completed some of the earliest boiling experiments with R1234yf. However, neither of these were for flow boiling in micro-fin tubes. The study by Park and Jung (2010) was for nucleate pool boiling while the one by Saitoh et al. (2011) was for flow boiling in a horizontal smooth tube. Only a few works exist for R1234yf flow boiling in micro-fin tubes. For example, Diani et al. (2015) and Mendoza-Miranda et al. (2015) and have experimentally investigated the heat transfer performance of R1234yf in micro-fin tubes. Diani et al. (2015) made measurements on a single tube and found that they compared well with heat transfer correlations from the literature. Mendoza-Miranda et al. (2015) measured the overall heat transfer performance of a shell-and-tube heat exchanger in an operating refrigerant cycle. They used micro-fin tube correlations from the literature and found that the heat transfer performance of a shell-and-tube heat exchanger with micro-fin tubes could be successfully modeled. Han et al. (2013) and Kedzierski and Park (2013) measured the flow boiling heat transfer characteristics of a R1234yf/lubricant and a R1234yf/R134a mixture, respectively, inside a micro-fin tube.

Currently, there are no published studies for measured flow boiling of R450A in a micro-fin tube. Mendoza-Miranda et al. (2016) recently used a model to predict the overall heat transfer for a shell-and-micro-fin tube evaporator with R450A on the micro-fin tube side. Gorgy (2016) presents pool boiling measurements with R450A.

Because of the relatively recent introduction of R1234yf and R450A, the availability of measured heat transfer data in a micro-fin tube in the literature is lacking for these refrigerants. Consequently, the present study provides local flow boiling heat transfer measurements for these two low-GWP refrigerants in a micro-fin tube for test conditions that are applicable for air conditioning applications.

2. Experimental apparatus

Fig. 1 shows a sketch of the experimental apparatus used to establish and measure convective boiling heat transfer coefficients. The experimental test facility consisted of two main systems: the refrigerant loop and the water loop. The refrigerant flow rate, pressure, and quality were fixed at the inlet to the test section. The water flow rate and the inlet temperature were fixed to establish the overall refrigerant quality change in the test section. The water temperature drop, the tube wall temperature, the refrigerant temperatures, pressures, and pressure drops were measured at several axial locations along the test section. These measurements were used to calculate the local heat-transfer coefficient for the micro-fin tube.

The test section consisted of a pair of 3.34 m long, horizontal tubes connected by a U-bend. A fixed test pressure was maintained by balancing the refrigerant duty between the subcooler, the test section, the preheater and the condensers. A magnetically coupled gear pump delivered the test refrigerant to the entrance of the test

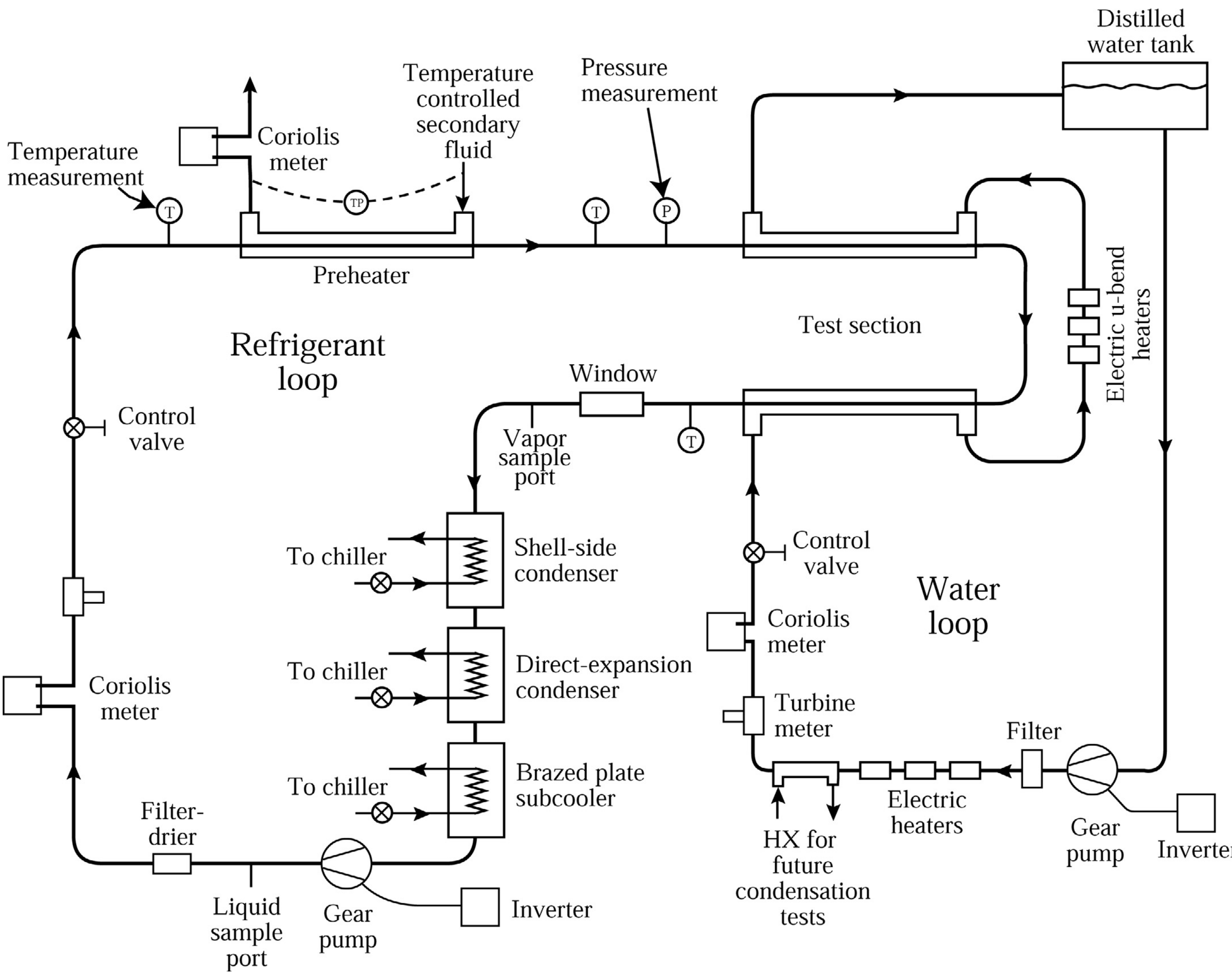

Fig. 1. Schematic of test rig showing counterflow arrangement.

section as saturated, near zero quality, liquid. Another magnetically coupled gear pump supplied a steady flow of water to the annulus of the test section. The inlet temperature of the water loop was held constant for each test with a water chilled heat exchanger and variable electric heaters. The refrigerant and water flow rates were controlled by varying the pump speeds using frequency inverters. Redundant flow rate measurements were made with Coriolis flowmeters and with turbine flowmeters for both the refrigerant and water sides.

Fig. 2 shows a cross section of the test section with a detail of the micro-fin tube geometry. The test refrigerant flowed inside a micro-fin tube, while distilled water flowed either in parallel flow or counterflow to the refrigerant in the annulus that surrounded the micro-fin tube. Having some tests in parallel flow and others in counterflow (as shown in Fig. 1) produced a broad range of heat fluxes at both low and high flow qualities. The annulus gap was 2.2 mm, and the micro-fin tube wall thickness was 0.3 mm. The micro fin tube had 60, 0.2 mm high fins that rifled down the axis of the tube at a helix angle (α) of 18° with respect to the tube axis. For this geometry, the cross sectional flow area was 60.8 mm^2, giving an equivalent smooth diameter (D_e) of 8.8 mm. The root diameter of the micro-fin tube was 8.91 mm. The inside-surface area per unit length of the tube was estimated to be 44.6 mm. The hydraulic diameter (D_h) was measured with a polar planimeter from a scaled drawing of the tube cross section and determined to be approximately 5.45 mm. The ratio of the inner surface area of the micro fin tube to the surface area of a smooth tube of the same D_e was 1.6.

Fig. 3 provides a detailed schematic of the test section. The annulus was constructed by connecting a series of tubes with 14 pairs of stainless steel flanges. This construction permitted the measurement of both the outer micro-fin wall temperature and the water temperature drop as discussed in the following two paragraphs. The design also avoided abrupt discontinuities such as unheated portions of the test section and tube-wall "fins" between thermopile ends.

Fig. 3 shows that thermocouple wires pass between 12 of the gasketed flange pairs to measure the refrigerant-tube wall temperature at ten locations on the top, side, and bottom of the tube wall. These locations were separated by 0.6 m on average, and they were located near the intersection of the shell flanges. In addition to these, thermocouples were also mounted next to the pressure taps near the middle of each test section length. The thermocouple junction was soldered to the outside surface and was sanded to a thickness of approximately 0.5 mm. The leads were strapped to a thin non-electrically-conducting epoxy layer on the wall for

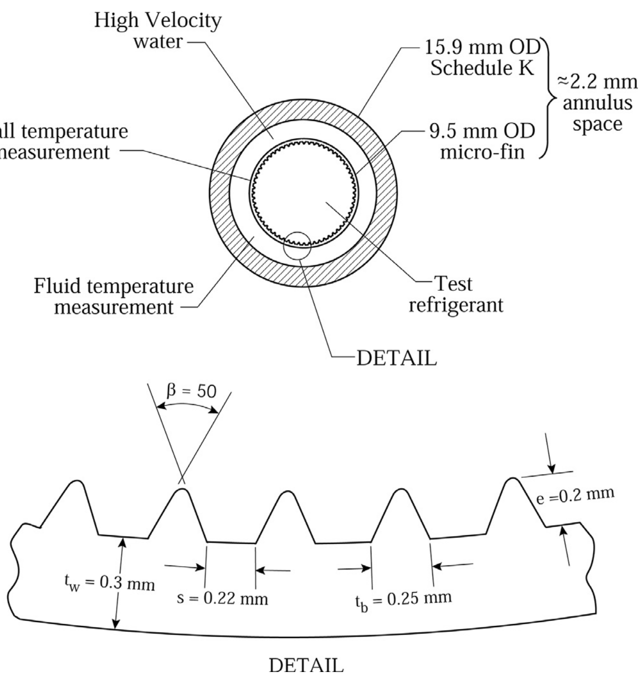

Fig. 2. Test section cross section.

a distance of 14.3 mm before they passed between a pair of the shell flanges. The wall temperature was corrected for a heat flux dependent fin effect. The correction was typically 0.05 K. Fig. 3 also shows that a chain of thermopiles was used to measure the water temperature drop between each flange location. Each thermopile consisted of ten thermocouples in series, with the ten junctions at each end evenly spaced around the circumference of the annulus. Because the upstream junctions of one thermopile and the downstream junctions of another enter the annulus at the same axial location (except at the water inlet and outlet), the junctions of the adjacent piles were alternated around the circumference. A series of Teflon half-rings attached to the inner refrigerant tube centered the tube in the annulus. The half-rings were circumferentially baffled to mix the water flow. Mixing was further ensured by a turbulent water Reynolds number (Kattan et al., 1995).

As shown in Fig. 3, six refrigerant pressure taps along the test section allowed the measurement of the upstream absolute pressure and five pressure drops along the test section. Two sets of two water pressure taps were used to measure the water pressure drop along each tube. Also, a sheathed thermocouple measured the refrigerant temperature at each end of the two refrigerant tubes, with the junction of each centered radially. Only the thermocouple at the inlet of the first tube was used in the calculations. The entire test section was wrapped with 5 cm of foam insulation to minimize heat transfer between the water and the ambient.

3. Measurements

Table 1 shows the expanded measurement uncertainty (U) of the various measurements along with the range of each test parameter in this study. The U was estimated with the law of propagation of uncertainty. All expanded measurement uncertainties are reported at the 95% confidence level. The estimates shown in Table 1 are median values of U for the correlated data. Saturated refrigerant properties were evaluated at the measured saturation pressure with the REFPROP (Lemmon et al., 2013) equation of state while using refrigerant-vendor proprietary fluid files for

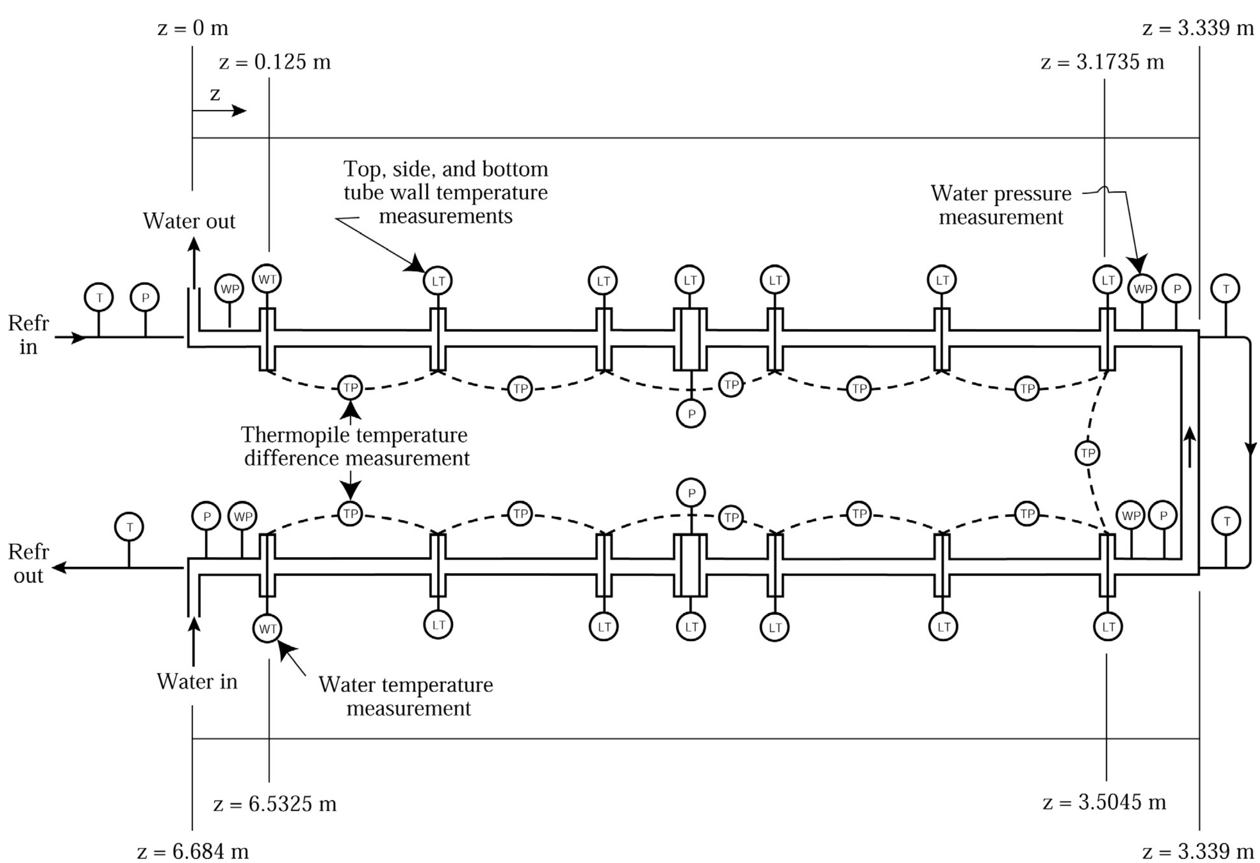

Fig. 3. Detailed schematic of test section (counterflow).

Table 1
Median estimated 95% relative expanded uncertainties for measurements (U).

Parameter	Minimum	Maximum	U %
G_r [kg m^{-2} s^{-1}]	96	318	2.0
T_s [K]	273.8	281.8	0.1 (0.3 K)
P [kPa]	273	369	1.5
T_w [K]	276.1	285.0	0.1 (0.4 K)
$\dot{m}_f$[kgs^{-1}]	0.006	0.019	2.0
T_f [K]	278.3	295.4	0.1
P_f [kPa]	200	110	1.0
q" [kW m^{-2}]	1.4	18.9	15
$(T_d - T_b)/T_b$	0	0.002	3.0
Nu	94	346	20
Re	2102	8242	4.0
Bo	0.000039	0.00049	16.0
Pr	3.5	4.0	2.0
P_s/P_c	0.07	0.11	2.0
x_q	0.03	0.87	8.0
ΔT_s [K]	0.96	5.41	0.44 K

R450A. Table 2 shows representative properties that were obtained from REFPROP for the fluids germane to this study. The left side of Table 2 shows properties that were evaluated for the average test conditions of each fluid, while the right side of the table provides properties that were evaluated at 277.6 K.

The convective boiling heat transfer coefficient based on the actual inner surface area ($h_{2\phi}$) was calculated as:

$$h_{2\phi} = \frac{q''}{T_w - T_s} \tag{1}$$

where the measured wall temperatures (T_w) were fitted to their axial position to reduce the uncertainty in the measurement.

Kedzierski and Kang (2017) provide the estimated expanded uncertainty of the wall temperature fit for all the measurements as a function of thermodynamic quality. The average uncertainty, at the 95% confidence level, of the fitted wall temperatures for the counterflow and the parallel flow data was approximately 0.42 K and 0.36 K, respectively. The median of the uncertainty in T_w as shown in Table 1 was approximately 0.4 K.

The water temperature (T_f) was determined from the measured temperature change obtained from each thermopile and the inlet water temperature measurement. The water temperature gradient (dT_f/dz) was calculated with second-order finite difference equations using the measured water temperatures and their locations along the tube length z. The water temperature gradients were then fitted with respect to the tube length. As a check on the water temperature gradient calculation, Fig. 4 shows that the measured water temperatures (open circles) typically agreed with the integrated fit of the water temperature gradient (solid line) to within 0.2 K.

The fitted, local, axial water temperature gradient (dT_f/dz), the measured water mass flow rate ($\dot{m}_f$), and the properties of the water were used to calculate the local heat flux (q") to the micro-fin tube based on the actual inner surface area:

$$q'' = \frac{\dot{m}_f}{p}\left(c_{p_f}\frac{dT_f}{dz} + \nu_f\frac{dP_f}{dz}\right) \tag{2}$$

where p is the wetted perimeter of the inside of the micro-fin tube. The specific heat (c_{pf}) and the specific volume (ν_f) of the water were calculated locally as a function of the water temperature. The water pressure gradient (dP_f/dz) was linearly interpolated between the pressure taps to the location of the wall thermocouples. The pressure gradient term was typically less than 3% of the temperature gradient term. The heat flux obtained by Eq. (2) was reduced by the amount of heat lost to the surroundings. The heat loss to the surroundings was obtained by calibration of single phase heat transfer tests and it was based on the temperature difference between the room and the test fluid. Typically, the heat loss correction was less than a 0.1% of that obtained from Eq. (2). Kedzierski and Kang (2017) provide the relative uncertainty of the heat flux measurement versus the heat flux. Overall, the uncertainty of the heat flux remains less than 40 % of the measured value, while the average uncertainty for the counterflow and the parallel flow data is approximately 7% and 20% of the measured value, respectively.

Fig. 5 shows example plots of the local heat flux as calculated from Eq. (2) versus thermodynamic quality for both cases when the water and the refrigerant are in counterflow and parallel flow, respectively. Both heat flux profiles are for R134a at an all-liquid Reynolds number (Re) of roughly 4418 and a refrigerant reduced pressure of approximately 0.09, which was evaluated at the exit of the test section. The discontinuity exhibited in the heat flux profiles is due to the change in refrigerant saturation temperature as caused by the adiabatic pressure drop in the bend that is used to transition from the first leg of the test section to the second leg. The decrease in the refrigerant saturation temperature causes an increase in the difference between the water and the refrigerant temperature, which leads to an increase in the local heat flux. For the counterflow case, the heat flux increases from approximately 1 kW m^{-2} at a quality near zero to approximately 14 kW m^{-2} at a quality slightly greater than 0.7. The parallel flow case has the opposite slope and a slightly different range of that for counterflow where the heat flux decreases from approximately 12 kW m^{-2} at a quality near 0.05 to approximately 1 kW m^{-2} at a quality of approximately 0.82.

The thermodynamic and transport properties were calculated with version 9.1 of REFPROP (Lemmon et al., 2013) while using enthalpy and pressure as inputs. The enthalpy of the refrigerant liquid at the inlet of the test section was calculated from its measured temperature and pressure. The subsequent increase in refrigerant enthalpy along the test section was calculated from the local heat flux and the measured refrigerant mass flow rate. The refrigerant pressures were measured at six pressure taps along the test section. The pressure was linearly interpolated between the taps. The refrigerant exiting the test section was held to approximately 277.6 K while the fluid entering the test section was near zero quality for all of the tests. Considering that the tests were done for quality ranges between near zero and slightly greater than 0.7, the saturation temperature of the test refrigerants decreased from roughly 282.0 K to 277.6 K for most tests due to the pressure drop. Because the temperature glide of R450A was less than 1 K, as shown in Table 2, the variation in saturation temperature during tests was similar to that for the single-component refrigerants R1234yf and R134a.

The local Nusselt number (Nu) was calculated using the hydraulic diameter and the heat transfer coefficient based on the actual inner surface area of the tube as:

$$Nu = \frac{h_{2\phi} D_h}{k_l} \tag{3}$$

Kedzierski and Kang (2017) present the relative uncertainty of the Nu as a function of the thermodynamic quality. The uncertainty of Nu was between roughly 10% and 40%. Measurements of Nu with uncertainties greater than 40% were discarded. For all qualities, the average uncertainty of Nu for the presented data was approximately 25% and 29% for counterflow and parallel flow,

Table 2
Representative properties from REFPROP (Lemmon et al., 2013).

Test fluid	Evaluated at average test conditions for each fluid			Evaluated at $T_s = 277.6$ K						
	T_d–T_b (K)	k_l (W m^{-1} K^{-1})	Pr	σ (mN m^{-1})	ρ_l (kg m^{-3})	ρ_v (kg m^{-3})	$[P_s]_{xq=0}$ (kPa)	c_p (J kg^{-1} K^{-1})	i_{fg} (KJ kg^{-1})	μ_l (μPa s)
R1234yf	0	0.070	3.5	8.85	1162.2	20.4	366.3	1306	160.39	197.31
R134a	0	0.090	3.8	10.8	1279.9	16.8	343.0	1354	195.17	251.86
R450A	0.64	0.084	4.0	11.4	1244.5	15.4	304.0	1339	185.62	249.45

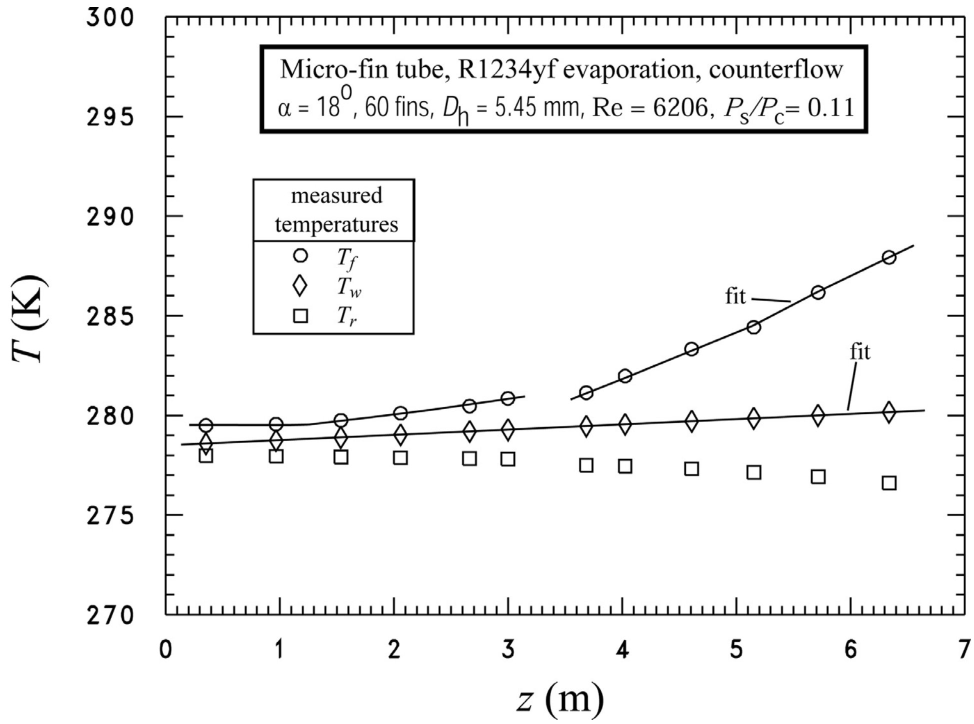

Fig. 4. Counterflow temperature profiles for a R1234yf test.

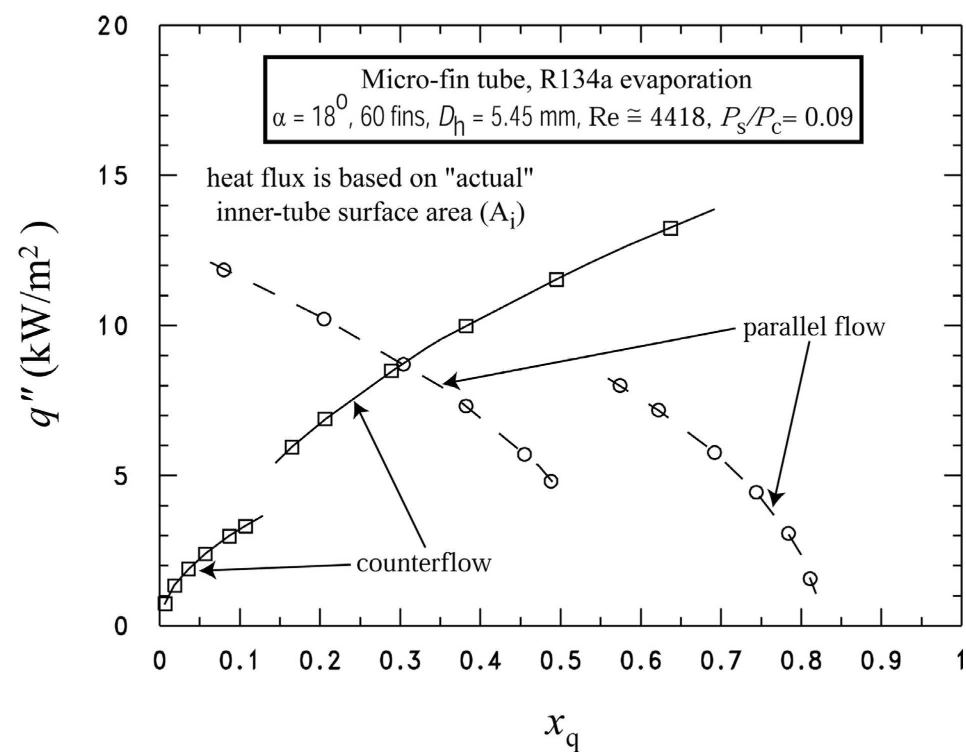

Fig. 5. Heat flux distribution for R134a.

respectively. The reported uncertainties are for the individual measurements. Reduction in the uncertainty can be achieved with repeat measurements for the same operating conditions. However, repeat measurements are difficult to obtain due to the chaotic nature of two-phase flow and the many fixed parameters that need to be matched between measurements. Hamilton et al. (2008) present a validation of the test apparatus and the test procedure using measurements from five different studies of five different micro-fin tubes and four different refrigerants from the literature. The validation consisted of using the Hamilton et al. (2008) model, that was developed using measurements from the present test apparatus, to predict most of these measurements to within ± 20%.

4. Results

4.1. Heat transfer measurements

The 756 data points generated in this study for R1234yf, R134a, and R450A are tabulated in Kedzierski and Kang (2017), which contains the Nusselt and all-liquid Reynolds numbers and other reduced data that are typically used to characterize flow boiling. Kedzierski and Kang (2017) also give the raw measurements including the heat flux and the wall and water temperatures and locations.

The measured local convective boiling Nusselt numbers (Nu) for R134a and R1234yf were compared to the pure-refrigerant (single component) version of the Hamilton et al. (2008) correlation:

$$Nu_p = 482.18\mathrm{Re}^{0.3}\mathrm{Pr}^{C_1}\left(\frac{P_s}{P_c}\right)^{C_2} Bo^{C_3}\left(-\log_{10}\frac{P_s}{P_c}\right)^{C_4} M_w{}^{C_5} \quad (4)$$

where

$$C_1 = 0.51x_q$$

$$C_2 = 5.57x_q - 5.21x_q^2$$

$$C_3 = 0.54 - 1.56x_q + 1.42x_q^2$$

$$C_4 = -0.81 + 12.56x_q - 11.00x_q^2$$

$$C_5 = 0.25 - 0.035x_q^2$$

Here, the all-liquid Reynolds number (Re), the Boiling number (Bo), the liquid Prandtl number (Pr), the reduced pressure (P_s/P_c), and the quality (x_q) are all evaluated locally at the saturation temperature. The all-liquid Reynolds number and the Nusselt number are based on the hydraulic diameter (D_h). The Nusselt number is also based on the actual inner surface area of the tube.

Kedzierski and Kang (2016) provide a correction factor for Eq. (4) to predict the flow boiling Nusselt Number (Nu) for mixtures of any number of refrigerants. This was done by multiplying the single-component Nusselt Number (Nu_p) by a modifier to predict multi-component mixtures:

$$Nu = Nu_p\left(1 - 36.23\left[\frac{T_d - T_b}{T_b}\right]e^{-0.007\mathrm{Re}Bo^{0.47}}\right) \quad (5)$$

where T_d and T_b are the dew-point and bubble-point temperatures, respectively, evaluated at the local saturation pressure and overall composition of the mixture. The T_d - T_b difference is commonly called the temperature glide of the mixture. Typically, large temperature glides cause concentration gradients that lead to heat transfer degradations as compared to what would be expected from a single-component prediction model (Kedzierski et al., 1992). Consequently, the bracketed term in Eq. (5) that multiplies Nu_p describes the mixture degradation effect, which is a function of temperature glide, Bo and Re. A single-component refrigerant would have zero temperature glide, which would result in the mixture degradation effect, represented by the bracketed term, being equal to one. Eq. (5) was used along with Eq. (4) to predict the Nu for R450A.

The flow map of Yu et al. (2002) for micro-fin tubes was used to determine that approximately 68% of the measurements were in annular or semi-annular flow with the remaining flow being in low quality intermittent flow. Manwell and Bergles (1990) suggest that the reason annular-like flow is a strong characteristic of micro-fin tubes is that the spiraling fins along the tube axis encourage wetting of the upper tube wall.

Fig. 6 shows a comparison between the boiling Nusselt numbers predicted with Eq. (5) for the micro-fin tube to those measured here for R1234yf, R134a, and R450A. The gray dashed lines of Fig. 6 are multi-use 95% confidence intervals on the mean prediction, which vary from ± 7 % of the prediction at a Nu of approximately 140 to approximately ± 3% for Nusselt numbers around 300. Eq. (5) predicts approximately 63% of the measured convective boiling Nusselt numbers for R1234yf, R134a, and R450A in the micro-fin tube to within approximately ± 20%. All of the R134a measurements are predicted to within 33% of the measurements while the R1234yf and the R450A predictions are within 50% of the measurements. Overall, the measurements for qualities less than 40% are predicted better than those for qualities greater than 40%. Nearly 70% of the predictions that lie outside of the ± 20% overprediction line are for qualities greater than 40%.

In an effort to obtain a better prediction of the present data set, a more complicated superposition flow boiling model of Daini et al. (2014) for micro-fin tubes was used and is shown in Fig. 7. Fig. 7 plots the measurements versus predicted values of the Nusselt number for R1234yf, R134a, and R450A using the same symbols to represent each fluid as was done in Fig. 6. Eq. (5) was applied to the Daini et al. (2014) model for R450A refrigerant and it accounted for less than a 4% adjustment to the prediction. The predictions appear to be more centered about the measurements; however, a smaller percentage (50%) of the measurements, as compared to the modified Hamilton et al. (2008) correlation (63%), are predicted to within ± 20%. For flow qualities less than 40%, the Hamilton et al. (2008) correlation predicted approximately 94% of the measurements to within ± 20%. In contrast, the Daini et al. (2014) model predicts roughly 35% of the measurements for qualities less than 40% to within ± 20%.

Some of the of cause of the 50% overprediction by the modified Hamilton et al. (2008) correlation for the R1234yf and R450A fluids may be due to a marginally larger uncertainty in the thermodynamic and transport fluid property predictions for these relatively new refrigerants as compared to R134a. For example, a recently developed viscosity correlation for R1234yf by Huber and Assael (2016) gives a viscosity that is approximately 3% larger than that given by REFPROP (Lemmon et al., 2013) in Table 2 for 277.6 K. However, even if it were assumed that the actual values for the liquid thermal conductivity, the liquid viscosity, and the critical pressure were 20% less, 10% less, and 10% greater than those provided by REFPROP, then the overprediction of the Hamilton et al. (2008) model would be reduced by only approximately 10%. Consequently, it is believed that it is not likely that errors in property predictions contribute significantly to the heat transfer overprediction.

This notwithstanding, if “corrections” to the property predictions as detailed above are applied to an approximate heat transfer property analysis, the analysis can be used to explain the difference between the R1234yf and R134a heat transfer coefficients. The present measurements show that the heat transfer coeffi-

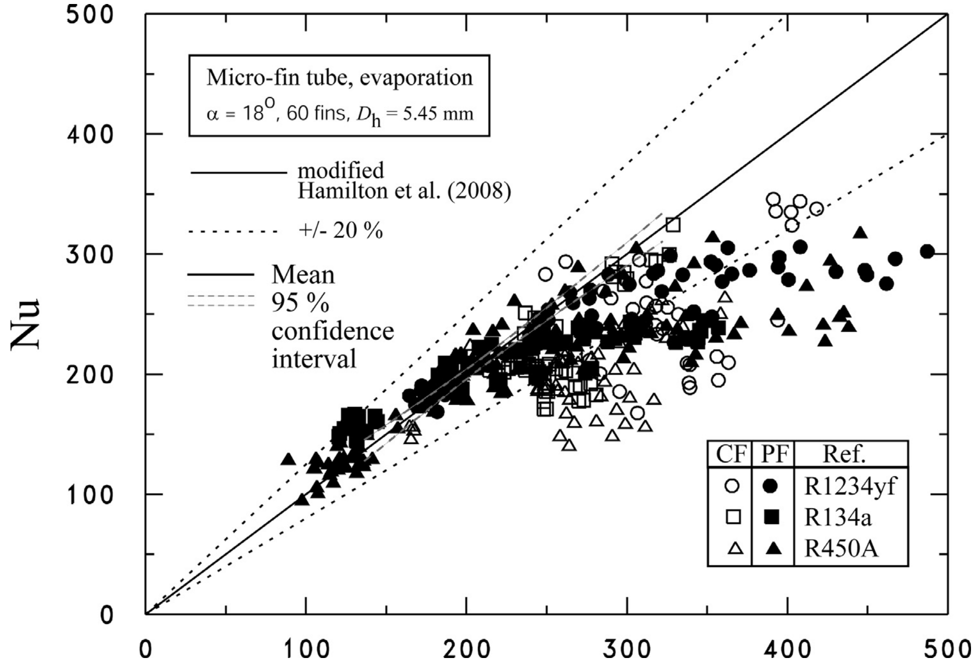

Fig. 6. Comparison between measured Nusselt numbers and those predicted by the modified Hamilton et al. (2008) correlation.

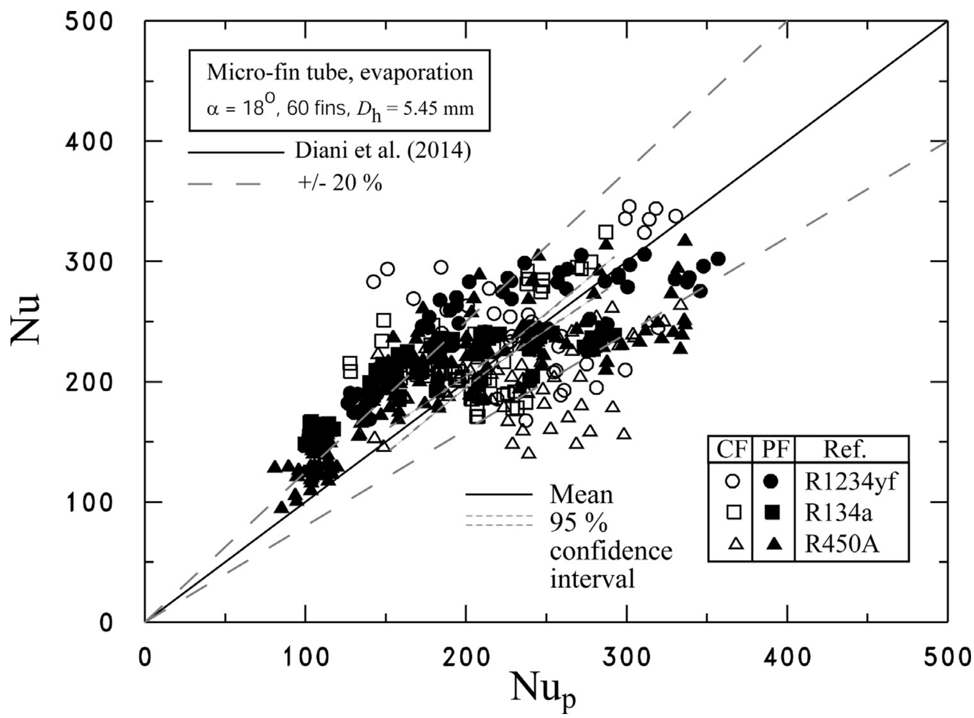

Fig. 7. Comparison between measured Nusselt numbers and those predicted by the Diani et al. (2014) correlation.

cient for R1234yf is, on average, 5% less than that for R134a. This difference is confirmed by the convective boiling measurements presented by Diani et al. (2015) for a micro-fin tube where the R1234yf heat transfer coefficient was shown to be approximately 8% less than that of R134a. However, if the convective property group $k_l^{0.6}(c_{pl}/\mu_l)^{0.4}\rho_l^{0.8}$ is calculated using REFPROP, as recommended by Kedzierski et al. (1992), to gauge the influence of convection for a fluid, the value for R1234yf is approximately 13% less than that for R134a. For equal values of latent heat of evaporation, the convective property group would give a good indication of the relative values of convective boiling for two fluids. However, as Table 2 shows, the latent heat of evaporation for R1234yf is approximately 18% less than that for R134a. Based on the fluid properties and the exponent on the Bo in Eq. (4), the R1234yf heat transfer coefficient should be approximately 16% less than that of R134a. For this case, "corrections" to properties could be used to bring the simple heat transfer property analysis and heat transfer measurements into better agreement by reducing the liquid thermal conductivity and increasing the liquid viscosity by approximately 8%. In a similar way, it can be shown that the relative heat

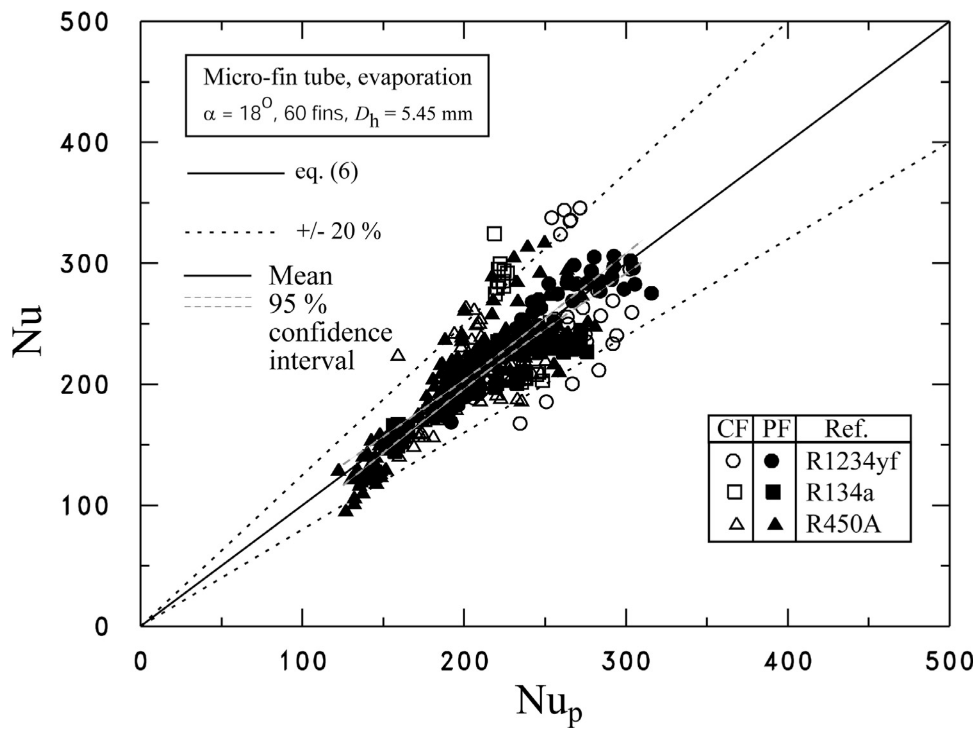

Fig. 8. Comparison between measured Nusselt numbers and those predicted by Eq. (6).

transfer measurements of R450A and R134a can be corroborated with an approximate analysis if the R450A liquid thermal conductivity and liquid viscosity are reduced and increased, respectively, by approximately 5% along with an average 4% mixture degradation effect.

The following measurement correlation was developed to have use of a more accurate representation of the data than Eq. (4) or the Diani et al. (2014) model for comparing the flow boiling heat transfer performance of the fluids at the same heat transfer conditions:

$$Nu_p = 6293\ \mathrm{Re}^{0.15}\mathrm{Pr}^{-1.43-3.54x_q}\left(\frac{P_s}{P_c}\right)^{-1.94x_q}Bo^{0.32} \tag{6}$$

Fig. 8 shows that Eq. (6) predicts approximately 91% of the measured convective boiling Nusselt numbers for R1234yf, R134a, and R450A in the micro-fin tube to within approximately ± 20%. The gray dashed lines of Fig. 8 are multi-use 95% confidence intervals on the mean prediction, which vary from ± 7% of the prediction at a Nu of approximately 140 to approximately ± 3% for Nusselt numbers around 300. Eq. (6) is not recommended for general use because the Prandtl number exponent is negative, which may be a consequence of the correlation compensating for inaccurate liquid thermal conductivity and liquid viscosity properties for the two low GWP refrigerants. This notwithstanding, Eq. (6) acceptably reproduces the convective boiling heat transfer measurements of this study so that a fair comparison can be made between fluids.

Representative plots of the heat transfer coefficient ($h_{2\phi}$) versus thermodynamic quality (x_q) for each of the three test fluids are given in Figs. 9 and 10 for counterflow and parallel flow configurations, respectively. The solid lines are predictions for the present micro-fin tube geometry, which were obtained from Eqs. (5) and (6). The symbols are the measured data points, while the shaded regions between the dashed lines provide the measurement uncertainty for a 95 % confidence level. For counterflow (Fig. 9), the uncertainty in the R1234yf and R134a heat transfer coefficients is shown to be roughly 900 W K^{-1} m^{-2} (± 24 %) for most of data for qualities greater than 10%. For these measurements, the uncertainty in the heat flux is the greatest contributor to the uncertainty in the heat transfer coefficient. The uncertainty in the R450A heat transfer coefficient is approximately 17% less than that of R1234yf and R134a for this particular example and is shown to be roughly 750 W K^{-1} m^{-2} (± 20%) for most of data for qualities greater than 35%. This result is primarily due to the R450A heat flux measurements generally having an approximately 17% smaller uncertainty than that for R1234yf and R134a measurements. For parallel flow with qualities less than 40%, the uncertainty in the heat transfer coefficients is essentially the same as quoted above for counterflow, i.e., ± 24% for R1234yf and R134a and ± 20% for R450A. For qualities greater than 40%, the uncertainty in the heat transfer coefficient is roughly 1600 W K^{-1} m^{-2} (± 40%). The large uncertainty in the heat transfer coefficient for parallel flow and the high-quality region is due to the large uncertainty in the measurement of a small heat flux and a small wall superheat.

Fig. 9 shows the local heat transfer coefficient for R1234yf, R134a, and R450A for $G_r \sim 200$ kg s^{-1} m^{-2} and $P_s/P_c \sim 0.1$ with counterflow between the refrigerant and the water. The P_s/P_c ratio is evaluated at the exit of the test section. As shown in Fig. 5, the counterflow condition provided increasing heat flux with increasing thermodynamic quality. As the convective boiling heat transfer coefficient is moderately dependent upon the heat flux, the increasing heat flux and the thinning liquid films on the wall cause the heat transfer coefficient to increase with respect to quality. Eq. (5), together with Eq. (6), is shown to predict both the R450A and the R134a measurements to within approximately 100 W K^{-1} m^{-2} (3–6%), for 75% and 50% of the measurements, respectively. Seventy-five percent of the R1234yf measurements are predicted to within approximately 200 W K^{-1} m^{-2}, or approximately ± 7%. Overall, the average difference between the measurements and the predictions for the counterflow measurements for R1234yf, R134a, and R450A was approximately ± 9%, ± 5%, and ± 2%, respectively. Average agreement within 2% indicates that the model is centered well about the data sets.

Fig. 10 shows the local heat transfer coefficient for R1234yf, R134a, and R450A for $G_r \sim 300$ kg s^{-1}m^{-2} and $P_s/P_c \sim 0.1$ with

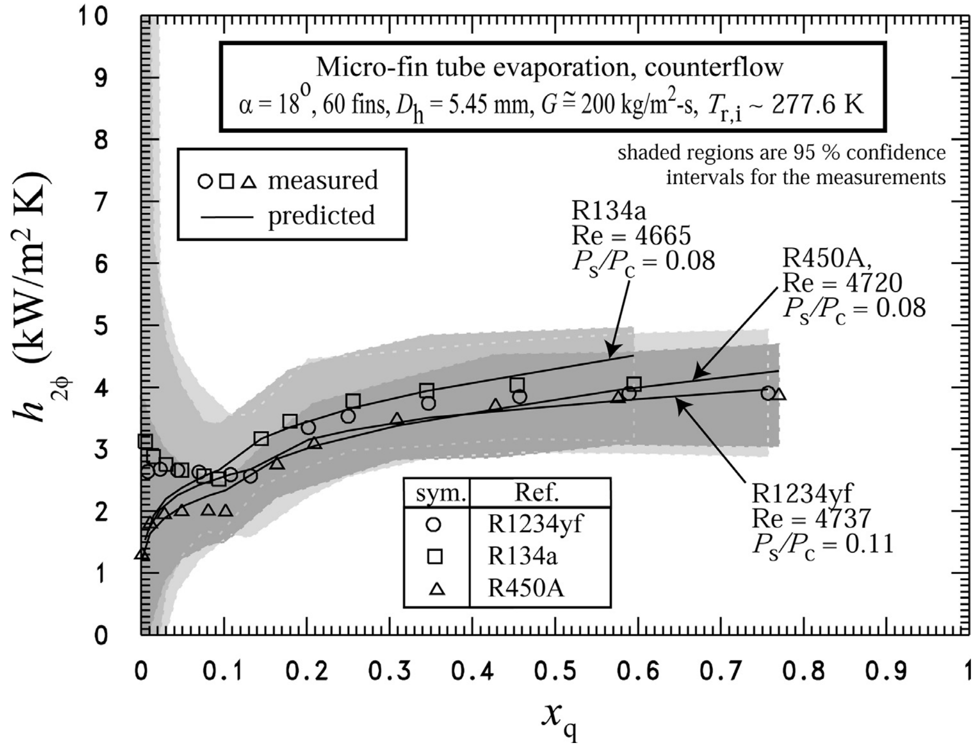

Fig. 9. Flow boiling heat transfer coefficient for micro-fin tube versus thermodynamic quality for R450A, R134a, and R1234yf (counterflow).

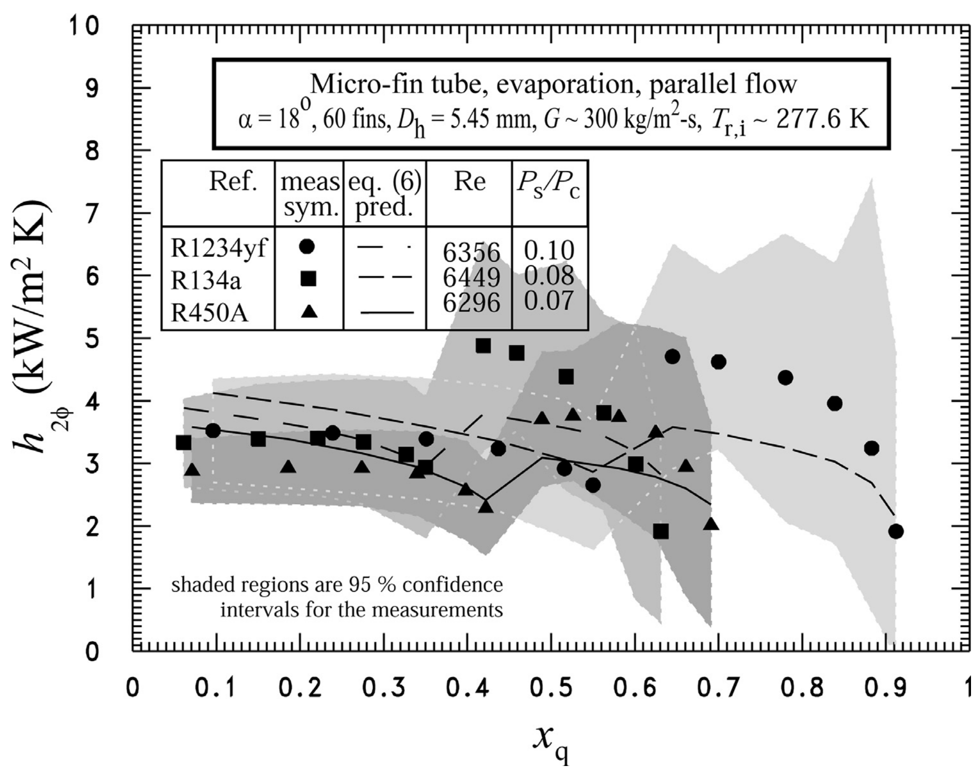

Fig. 10. Flow boiling heat transfer coefficient for micro-fin tube versus thermodynamic quality for R450A, R134a, and R1234yf (parallel flow).

parallel flow between the refrigerant and the water. As shown in Fig. 5, the parallel flow condition provided decreasing heat flux with increasing thermodynamic quality. Because of the high heat flux for qualities less than 20%, it is likely that nucleate boiling provides a larger contribution to the total heat transfer than it is for the counterflow condition, thus contributing to the large heat transfer coefficient for the low-quality region. For qualities larger than 20%, the effects of decreasing heat flux and the thinning liquid films on the wall cause the heat transfer coefficient to moderately decrease with respect to quality. Eq. (5) with Eq. (6) is shown to predict the heat transfer coefficient for the example parallel flow case to within 1100 W K^{-1} m^{-2} for the R1234yf and

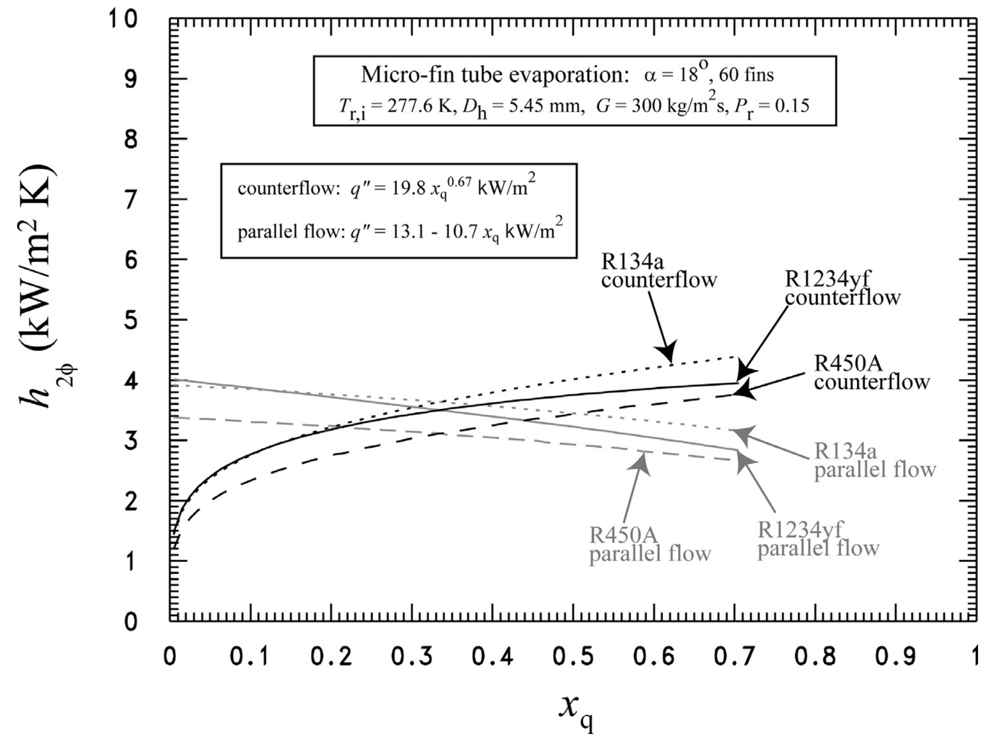

Fig. 11. Flow boiling heat transfer coefficient versus thermodynamic quality for test refrigerants.

the R134a measurements. The best predictions are achieved for the lower qualities exhibiting the smallest deviations from the measurements of 100 W K^{-1} m^{-2} and 10 W K^{-1} m^{-2} for R1234yf and R134a, respectively. This is also true for the best R450A predictions, which are within approximately 50 W K^{-1} m^{-2} (2%) of the measurements for a quality of roughly 40%. The maximum deviation between Eq. (5) predictions and the measurements for R450A is approximately 800 W K^{-1} m^{-2}, or approximately ± 27%. Overall, the average difference between the measurements and the predictions for the parallel flow measurements for R1234yf, R134a, and R450A was approximately ± 4%, ± 1%, and ± 1%, respectively.

The main purpose of Figs. 9 and 10 was to compare Eq. (5) predictions to the measurements for each fluid at as similar as conditions as the present data set would allow. Even though the measurements were compared at nearly the same mass velocity, 200 kg s^{-1} m^{-2} for Fig. 9 and 300 kg s^{-1} m^{-2} for Fig. 10, the local heat flux could vary significantly between fluids. For Fig. 9 example, the heat flux for R450A varied from approximately 0.3 kW m^{-2} to approximately 18 kW m^{-2}, while that for R1234yf varied from approximately 0.3 kW m^{-2} to 11 kW m^{-2}. This illustrates that the maximum heat flux for the R450A counterflow data set example was approximately 64% larger than that for R1234yf, which accentuated the difference in the measured heat transfer coefficients between the two fluids. For this reason, it is important to use a validated model to compare the performance of the fluids at identical conditions in order to establish a fair comparison of heat transfer performance.

Fig. 11 uses Eq. (5) to illustrate the relative heat transfer performance of R1234yf, R134a, and R450A versus quality for the same saturated refrigerant inlet temperature ($T_{r,i}$ = 277.6 K), and the same refrigerant mass flux (G_r = 300 kg m^{-2} s^{-1}) for the present micro-fin tube geometry. Both counterflow and parallel flow conditions are shown. The counterflow heat flux is approximated with $q'' = 19.8x_q^{0.67}$kW m^{-2}, while the parallel flow is approximated with $q'' = (13.1 - 10.7x_q)$kW m^{-2}. The heat flux profiles with respect to quality that were used to calculate the heat transfer coefficient are approximately equivalent to those shown in Fig. 5 and adjusted to ensure that they provide the same total heat over the plotted quality range. Three different line styles for each flow condition are used to represent the predictions for the three different test fluids as labeled.

In general, for counterflow, Fig. 11 predictions show that the boiling heat-transfer coefficient rapidly increases with increasing quality for qualities less than 20%. For quality ranges between 20% and 70%, the rate of increase in the heat transfer coefficient with respect to increasing quality is roughly a fourth of that for qualities less than 10%. For parallel flow, the heat transfer coefficient for all the fluids decreases with increasing quality in response to the decreasing heat flux with respect to increasing quality. For the example case presented here, the heat transfer coefficient for R1234yf is, on average, approximately 5% less than the heat transfer coefficient for R134a for qualities between 10% and 70% for both counterflow and parallel flow conditions. For both counterflow and parallel flow, the R1234yf heat transfer coefficient is nearly the same as that for R134a for qualities less than 20%. As the quality increases beyond 20%, the R1234yf heat transfer coefficient becomes increasingly smaller than that for R134a being approximately 10% less than that for R134a at a quality of 70%. As previously discussed, fluid properties shown in Table 2 would indicate that the difference between heat transfer coefficient for R1234yf and R134a should be larger than that which was measured. For the example case presented here, the heat transfer coefficient for R450A is, on average, approximately 15% less than the heat transfer coefficient for R134a for the entire illustrated quality range for both counterflow and parallel flow conditions. The smaller heat transfer coefficient of R450A as compared to that of R134a is primarily due to the mixture degradation effect, as calculated by the bracketed right-side of Eq. (5), being on average 0.96 as compared to 1 for R134a, and the liquid thermal conductivity of R450A being approximately 7% less than that for R134a. The mixture degradation fac-

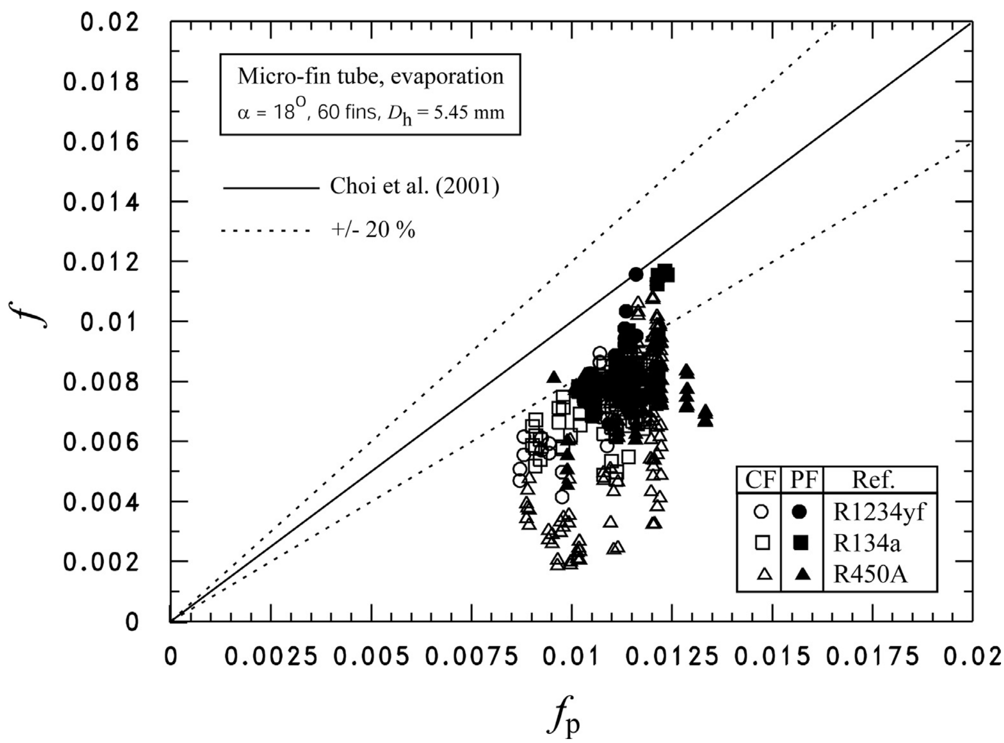

Fig. 12. Comparison between measured Fanning friction factors and those predicted by Choi et al. (2001).

tor reduces the single component prediction by an amount that is required to account for the mixture degradation effects.

At low qualities, because of the high heat fluxes produced by parallel flow heating and the low heat fluxes produced by counterflow heating (and vice-versa for high qualities), Fig. 11 can be used to illustrate the influence of heat flux on the convective flow boiling for the micro-fin tube. Jung et al. (1989) have performed a similar investigation for a smooth tube. Jung et al. (1989) have shown that, for an electrically heated test apparatus, and for qualities less than roughly 30%, the flow boiling heat transfer coefficient is strongly dependent on the heat flux. They suggest that the heat flux dependence is due to the presence of nucleate boiling. Jung et al. (1989) also show that, despite a wide variation in heat fluxes (10 kWm^{-2} to 45 kWm^{-2}), the data collapse into a single curve for qualities greater than roughly 30%. They use this behavior to identify the suppression of nucleate boiling as occurring at the point where the heat flux dependence of the heat transfer coefficient vanishes and where convective boiling begins to dominate. For the present micro-fin tube, Fig. 11 supports the Jung et al. (1989) analysis for qualities less than 30% where larger heat transfer coefficients are associated with the larger heat fluxes. For example, at a quality of 0.05, an increase in the heat flux from roughly 2.7 kWm^{-2} (counterflow) to 12.6 kWm^{-2} (parallel flow) caused an increase in the heat transfer coefficient of over 50%. In comparison, for a quality of 0.7, an increase in the heat flux from roughly 5.6 kWm^{-2} (parallel flow) to 15.6 kWm^{-2} (counterflow) caused roughly a 43% increase in the heat transfer coefficient. The heat flux dependence in the convective region contradicts the Jung et al. (1989) observation of the convective region heat transfer coefficient being independent of heat flux. However, the heat flux dependence of the flow boiling heat transfer coefficient in the convective region for *fluid heated* data has been previously noted by Kaul et al. (1996). This emphasizes the importance of fluid heated measurements for providing an accurate representation of real world heat exchange equipment and that electrically heated boiling measurements should be used with caution (Darabi et al., 1999).

5. Fanning friction factor measurements

Tabulated Fanning friction factor measurements that correspond to the heat transfer measurements are provided in Kedzierski and Kang (2017). Fanning friction factor (f) measurements were made following the procedure outlined by Kedzierski and Goncalves (1999):

$$f = \frac{D_h}{(\nu_o + \nu_i)\Delta L}\left(\frac{(P_i - P_o)}{G^2} - (\nu_o - \nu_i)\right) \quad (7)$$

where the specific volume of the fluid (ν) was calculated from the thermodynamic quality weighted average of the liquid and vapor specific volumes for the exit (subscript o) and the inlet (subscript i) of each incremental length (ΔL). The P_i and the P_o are saturation pressures for the inlet and exit of the increment, respectively. The mass velocity (G) is the total liquid and vapor mass flow rate per cross sectional flow area. The hydraulic diameter (D_h) that was used was 5.45 mm.

Choi et al. (2001) present the following two-phase friction factor correlation for the micro-fin tube as:

$$f_p = 0.00506\mathrm{Re}^{-0.0951}K_f^{0.1554} \quad (8)$$

The predicted friction factor (f_p) is based on the all liquid Reynolds number (Re), and the two-phase number as defined (K_f) by Pierre (1964)

$$K_f = \frac{\Delta x_q i_{fg}}{g\Delta L} \quad (9)$$

Here, the quality change from the inlet to the exit of the increment is Δx_q, and the acceleration of gravity constant is g.

Fig. 12 shows a comparison between the measured Fanning friction factors for the micro-fin tube to those predicted with the Choi

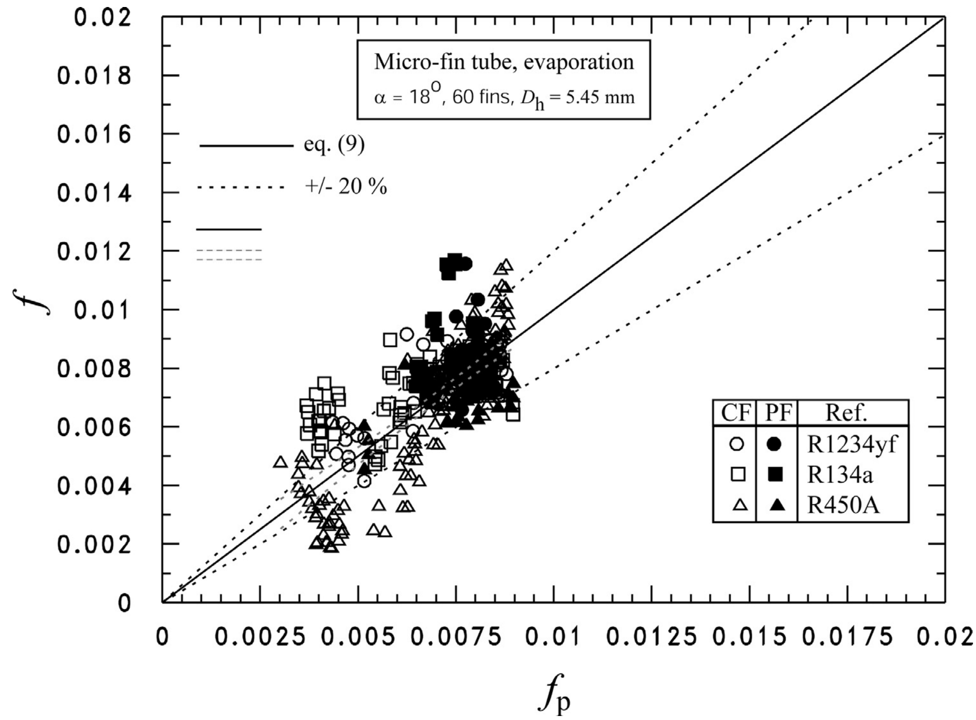

Fig. 13. Comparison between measured Fanning friction factors and those predicted by Eq. (9).

et al. (2001) correlation for the R1234yf, R134a, and R450A test refrigerants. Only measurements with an uncertainty less than 40% as given in Kedzierski and Kang (2017) were used in the comparison. The solid line shows Eq. (8) prediction. The dashed lines represent predictions that are ± 20% of the measured friction factors. The comparison shows that approximately 92% of the measurements are overpredicted by more than 20%.

Because of the relatively poor prediction capabilities of Eq. (8) a new correlation was developed for the prediction of the Fanning friction factor for the micro-fin tube:

$$f_p = 0.0337\mathrm{Re}^{0.24-0.63x_q}\mathrm{Bo}^{0.46-0.82x_q+0.19x_q^2} \tag{10}$$

Fig. 13 compared the measured Fanning friction factors to predictions using Eq. (10). The gray dashed lines of Fig. 13 are multi-use 95% confidence intervals on the mean prediction, which vary from ± 17% of the prediction at a f of approximately 0.0035 to approximately ± 3% for friction factors around 0.0085. Eq. (10) predicts approximately 76% of the measured two-phase friction factors for R1234yf, R134a, and R450A in the micro-fin tube to within approximately ± 20%.

6. Conclusions

Local convective boiling heat transfer measurements for R134a and two low-GWP refrigerants (R1234yf and R450A) in a fluid heated micro-fin tube were presented. The new correlation for convective boiling Nusselt numbers for all the test refrigerants was developed that predicted approximately 90% of the measurements to within ± 20%. Measured Fanning friction factors were also presented and compared to a new predictive correlation that was a function of the all-liquid Reynolds number, the local thermodynamic quality, and the Boiling number. The developed Fanning friction factor correlation predicted approximately 76% of the measured two-phase friction factors for R1234yf, R134a, and R450A in the micro-fin tube to within approximately ± 20%.

In general, the measured boiling heat-transfer coefficient increased with increasing qualities when the local heat flux increased with respect to quality. In contrast, for decreasing heat flux with respect to increasing quality, the measured heat transfer coefficient was relatively constant. The heat transfer coefficient of the three test fluids were compared at the same heat flux, saturated refrigerant temperature, and refrigerant mass flux by using the developed correlation. The resulting example comparison showed that the heat transfer performance of R450A and R1234yf were, on average, 15% less and 5% less than that of the R134a, respectively. The greater heat transfer performance of R134a was due in part to its larger convective property group, and latent heat of vaporization as compared to R1234yf and R450A. In addition, R450A experienced an additional loss in flow boiling heat transfer, as compared to that of R134a, due to its small 0.64 K temperature glide.

Acknowledgments

This work was funded by NIST. The authors thank the following for their constructive criticism of the first draft of the manuscript: P. Domanski, and B. Dougherty from NIST, and Ki-J. Park from the Korea Atomic Energy Research Institute. Thanks also go to Wolverine Tube, Inc., for supplying the Turbo-A, micro-fin tube for the test section, and to Chemours and Honeywell for supplying the test refrigerants and the equation of state parameters for REFPROP.

References

Choi, J.Y., Kedzierski, M.A., Domanski, P.A., 2001. Generalized Pressure Drop Correlation for Evaporation and Condensation in Smooth and Micro-fin Tubes. IIF-IIR Commission B1, Paderborn, Germany, pp. B4.9–B4.16.
Darabi, J.D., Ohadi, M.M., Fanni, M.A., Dessiatoun, S.V., Kedzierski, M.A., 1999. Effect of heating boundary conditions on pool boiling experiments. HVAC&R Res. 5 (4), 283–296.
Diani, A., Mancin, S., Rossetto, L., 2015. Flow boiling heat transfer of R1234yf inside a 3.4 mm ID microfin tube. Exp. Thermal Fluid Sci. 66, 127–136.
Diani, A., Mancin, S., Rossetto, L., 2014. R1234ze(E) flow boiling inside a 3.4 mm ID microfin tube. Int. J. Refrig. 47, 105–119.
Directive, 17 May 2006. Relating to emissions from air-conditioning systems in motor vehicles & amending council directive 70/156/EC. Off. J. Eur. Union 49 (L 161), 12–18.

Gorgy, E., 2016. Nucleate boiling of low GWP refrigerants on highly enhanced tube surface transfer. Int. J. Heat Mass Transf. 96, 660–666.
Hamilton, L.J., Kedzierski, M.A, Kaul, M.P., 2008. Horizontal convective boiling of pure and mixed refrigerants within a micro-fin tube. J. Enhanced Heat Transf. 15 (3), 211–226.
Han, X., Li, P., Yuan, X., Wang, Q., Chen, G., 2013. The boiling heat transfer characteristics of the mixture HFO-1234yf/oil inside a micro-fin tube. Int. J. Heat Mass Transf. 67, 1122–1130.
Honeywell, 2014, https://www.honeywell-refrigerants.com/europe/wp-content/uploads/2015/03/Solstice-N13-TDS-141027-LR-vF.pdf
Huber, M.L., Assael, M.J., 2016. Correlations for the Viscosity of 2,3,3,3-Tetrafluoroprop-1-ene (R1234yf) and trans-1,2,2,2-Tetrafluoropropene (R1234ze(E)). Int. J. Refrig. 71, 39–45.
IPCC, 2013, Climate Change 2013: The Physical Science Basis. Contribution of Working Group I to the Fifth Assessment Report of the Intergovernmental Panel On Climate Change. In: Stocker, T.F., Qin, D., Plattner, G.-K., Tignor, M., Allen, S.K., Boschung, J., et al. (Eds.). Cambridge University Press, Cambridge, United Kingdom New York, NY, USA, p. 1535. doi:10.1017/CBO9781107415324.
Kattan, N., Favret, D., Thome, J.R., 1995. R-502 and two near-azeotropic alternatives: part 1 - in tube flow-boiling tests. ASHRAE Trans. 101 (1), 491–508.
Kaul, M.P., Kedzierski, M.A., Didion, D.A., 1996. Horizontal Flow Boiling of Alternative Refrigerants within a Fluid Heated Micro-Fin Tube. In: Manglik, R.M., Kraus, A.D. (Eds.), Process, Enhanced, and Multiphase Heat Transfer: A Festschrift for A. E. Bergles. Begell House, Inc., New York, pp. 167–173.
Kedzierski, M.A., Kang, D.Y., 2017. Horizontal Convective Boiling of R1234yf, R134a, and R450A Within a Micro-Fin Tube; Extensive Measurement and Analysis. NIST Technical Note 1966, U.S. Department of Commerce, Washington, D.C.
Kedzierski, M.A., Kang, D.Y., 2016. Horizontal convective boiling of R448A, R449A, and R452B within a micro-fin tube. Sci. Technol. Built Environ. 22 (8), 1090–1103.
Kedzierski, M.A., Park, K.J., 2013. Horizontal convective boiling of R134a, R1234yf/R134a, and R1234ze(E) within a micro-fin tube. J. Enhanced Heat Transf. 20 (4), 333–346.
Kedzierski, M.A., Goncalves, J.M., 1999. Horizontal convective condensation of alternative refrigerants within a micro-fin tube. J. Enhanc. Heat Transf. 6 (2-4), 161–178.
Kedzierski, M.A., Kim, J.H., Didion, D.A., 1992. Causes of the apparent heat transfer degradation for refrigerant mixtures. In: Kim, J.H., Nelson, R.A., Hashemi, A. (Eds.), Two-Phase Flow and Heat Transfer, HTD Vol. 197. ASME, New York, pp. 149–158 Vol. 197.
Kim, Y., Seo, K., Chung, J., 2002. Evaporation heat transfer characteristics of R-410A in 7 and 9.52 mm smooth/micro-fin tubes. Int. J. Refrig. 25 (6), 716–730.
Kyoto Protocol 1997. United Nations Framework Convention on Climate Change. United Nations (UN), New York, NY, USA.
Lemmon, E.W., Huber, M.L., McLinden, M.O., 2013. NIST Standard Reference Database 23 (REFPROP), Version 9.1. Private Communications with McLinden, National Institute of Standards and Technology, Boulder, CO.
Jung, D.S., McLinden, M., Radermacher, R., 1989. Measurement Techniques for Horizontal Flow Boiling Heat Transfer with Pure and Mixed Refrigerants. Exp. Heat Transf. 2, 237–255.
Manwell, S.P., Bergles, A.E., 1990. Gas-liquid flow patterns in refrigerant-oil mixtures. ASHRAE Trans. 96 (2), 456–464.
Mendoza-Miranda, J.M., Mota-Babilonib, A., Navarro-Esbríc, J., 2016. Evaluation of R448A and R450A as low-GWP alternatives for R404A and R134a using a micro-fin tube evaporator model. Appl. Thermal Eng. 98 (5), 330–339.
Mendoza-Miranda, J.M., Ramirez-Minguela, J.J., Munoz-Carpio, V.D., Navarro-Esbri, J., 2015. Development and validation of a micro-fin tubes evaporator model using R134a and R1234yf as working fluids. Int. J. Refrig. 50, 32–43.
Montreal Protocol 1987. Montreal Protocol on Substances that Deplete the Ozone Layer. United Nations (UN), New York, NY, USA (1987 with subsequent amendments)
Myhre, G., Shindell, D., Bréon, F.-M., Collins, W., Fuglestvedt, J., Huang, J., Koch, D., Lamarque, J.-F., Lee, D., Mendoza, B., Nakajima, T., Robock, A., Stephens, G., Takemura, T., Zhang, H., 2013. Anthropogenic and Natural Radiative Forcing Supplementary Material. In: Stocker, T.F., Qin, D., Plattner, G.-K., Tignor, M., Allen, S.K., Boschung, J., et al. (Eds.), Climate Change 2013: The Physical Science Basis. Contribution of Working Group I to the Fifth Assessment Report of the Intergovernmental Panel On Climate Change Available from www.climatechange2013.org and www.ipcc.ch.
Olivier, J.A., Liebenberg, L., Kedzierski, M.A., Meyer, J.P., 2004. Pressure drop during refrigerant condensation inside horizontal smooth, helical micro-fin, and herringbone micro-fin tubes. J. Heat Transf. 126 (5), 687–696.
Park, K.-J., Jung, D., 2010. Nucleate boiling heat transfer coefficients of R1234yf on plain and low fin surfaces. Int. J. Refrig. 33, 553–557.
Pierre, B., 1964. Flow resistance with boiling refrigerants-part 1. ASHRAE J. 6 (9), 58–65.
Saitoh, S., Dang, C., Nakamura, Y., Hihara, E., 2011. Boiling heat transfer of HFO-1234yf flowing in a smooth small-diameter horizontal tube. Int. J. Refrig. 34, 1846–1853.
Seo, K., Kim, Y., 2000. Evaporation heat transfer and pressure drop of R-22 in 7 and 9.52 mm smooth/micro-fin tubes. Int. J. Heat Mass Transf. 43 (16), 2869–2882.
Webb, R.L., Kim, N-H., 2005. Principles of Enhanced Heat Transfer, 2nd ed., Taylor & Francis, New York.
Wellsandt, S., Vamling, L., 2005. Evaporation of R134a in a horizontal herringbone microfin tube: heat transfer and pressure drop. Int. J. Refrig. 28 (6), 889–900.
Yu, M., Lin, T., Tseng, C., 2002. Heat transfer and flow pattern during two-phase flow boiling of R-134a in horizontal smooth and micro-fin tubes. Int. J. Refrig. 25 (6), 789–798.
Yun, R., Kim, Y., Seo, K., Kim, H., 2002. A generalized correlation for evaporation heat transfer of refrigerants in micro-fin tubes. Int. J. Heat Mass Transf. 45 (10), 2003–2010.